www.elsevier.com/locate/jmbbm

Diffusion profile of macromolecules within and between human skin layers for (trans) dermal drug delivery

Anne M. Römgens, Dan L. Bader, Joke A. Bouwstra, Frank P.T. Baaijens, Cees W.J. Oomens

PII: S1751-6161(15)00212-X
DOI: http://dx.doi.org/10.1016/j.jmbbm.2015.06.019
Reference: JMBBM1513

To appear in: *Journal of the Mechanical Behavior of Biomedical Materials*

Received date: 23 March 2015
Revised date: 12 June 2015
Accepted date:
16 June 2015

Cite this article as: Anne M. Römgens, Dan L. Bader, Joke A. Bouwstra, Frank P.T. Baaijens, Cees W.J. Oomens, Diffusion profile of macromolecules within and between human skin layers for (trans)dermal drug delivery, *Journal of the Mechanical Behavior of Biomedical Materials,* http://dx.doi.org/10.1016/j.jmbbm.2015.06.019

Diffusion profile of macromolecules within and between human skin layers for (trans)dermal drug delivery

Anne M. Römgens[a], Dan L. Bader[a,b], Joke A. Bouwstra[c], Frank P.T. Baaijens[a], Cees W.J. Oomens[a]

[a]Soft Tissue Biomechanics and Engineering, Department of Biomedical Engineering, Eindhoven University of Technology, P.O. Box 513, 5600 MB Eindhoven, the Netherlands.
[b]Faculty of Health Sciences, University of Southampton, Southampton SO17 1BJ, UK.
[c]Division of Drug Delivery Technology, Leiden Academic Centre for Drug Research, Leiden University, P.O. Box 9502, 2300 RA Leiden, the Netherlands.

Corresponding author: A.M. Römgens, Soft Tissue Biomechanics and Engineering, Department of Biomedical Engineering, Eindhoven University of Technology, PO Box 513, 5600 MB Eindhoven, The Netherlands. Tel.: +31402475415, E-mail address: a.m.romgens@tue.nl

Abstract

Delivering a drug into and through the skin is of interest as the skin can act as an alternative drug administration route for oral delivery. The development of new delivery methods, such as microneedles, makes it possible to not only deliver small molecules into the skin, which are able to pass the outer layer of the skin in therapeutic amounts, but also macromolecules. To provide insight into the administration of these molecules into the skin, the aim of this study was to assess the transport of macromolecules within and between its various layers. The diffusion coefficients in the epidermis and several locations in the papillary and reticular dermis were determined for fluorescein dextran of 40 and 500 kDa using a combination of fluorescent recovery after photobleaching experiments and finite element analysis. The diffusion coefficient was significantly higher for 40 kDa than 500 kDa dextran, with median values of 23 and 9 $\mu m^2/s$ in the dermis, respectively. The values only marginally varied within and between the papillary and reticular dermis. For the 40 kDa dextran, the diffusion coefficient in the epidermis was twice as low as in the dermis layers. The adopted method may be used for other macromolecules, which are of interest for dermal and transdermal drug delivery. The knowledge about diffusion in the skin is useful to optimize (trans)dermal drug delivery systems to target specific layers or cells in the human skin.

Keywords

Diffusion coefficient; fluorescent recovery after photobleaching; scanning microphotolysis; targeted drug delivery; human skin

1. Introduction

(Trans)dermal administration is of interest for the delivery of drugs that cannot be administered orally, due to e.g. a strong first-pass effect, or have the skin as the target. The administration of vaccines is an example for which the dermal route may offer several advantages. By delivering a vaccine into the skin, the required dose to achieve a sufficient high immune response may be reduced when compared to conventional methods (Chen et al., 2011, 2010; Fernando et al., 2010; Gelinck et al., 2009; Quan et al., 2010). Multiple techniques to deliver antigens or other macromolecular drugs into the skin are currently in development, such as microneedles or microjet systems (Arora et al., 2008; van der Maaden et al., 2012). These techniques are necessary to overcome the skin barrier provided by the stratum corneum, the upper layer of the epidermis. However, to target specific layers of the skin, it is important to obtain insight in the transport of these molecules in the skin layers. This knowledge can be used to improve the design of delivery systems and to optimise delivery strategies.

The delivery and transport of fluorescent molecules in the skin has been previously visualized (Bal et al., 2010; Chen et al., 2012; Grams et al., 2004; Prow et al., 2010; Raphael et al., 2010), although the diffusion coefficient was not quantitatively determined. This parameter is essential to describe the passive transport of a molecule in a material and is dependent on both the properties of the diffusing molecule and the material through which it diffuses. In some previous studies, the diffusion coefficient of various model compounds in skin of different species was determined (Anissimov et al., 2012; Cornelissen et al., 2008; Hanh et al., 2001; Liu et al., 2013; Raphael et al., 2013; Wonglertnirant et al., 2010; Xing et al., 2009). Most of these studies report a single value of the diffusion coefficient for a single skin layer. For example, Cornelissen et al. (2008) measured the diffusion in human epidermis and Anissimov et al. (2012) in the stratum corneum. However, the diffusion coefficient may not only vary between skin layers, but also within the layers of the skin. This was shown in porcine dermis for a small molecule which has the property to extend the imaging depth using micro-Raman spectroscopy (Liu et al., 2013), and for a macromolecule in murine skin layers using confocal microscopy in combination with computational analyses (Raphael et al., 2013). However, for macromolecules and species with a thicker skin, like humans, these methods are not feasible due to the limitations in the imaging depth. To facilitate the development of (trans)dermal delivery systems, information on the specific diffusion properties of the human skin layers is essential. Indeed previous studies have reported differences in skin properties between species, including permeability and structure (Pasparakis et al., 2014; Scott et al., 1991), suggesting that diffusion coefficients in the various skin layers may be significantly different from

those measured in murine skin. To our knowledge, the variation in diffusion coefficient within and between human skin layers is currently unknown.

A possible method to determine the diffusion coefficient within the human skin is fluorescent recovery after photobleaching (FRAP, also referred to by video-FRAP or scanning microphotolysis) (Deschout et al., 2014). With FRAP, the entire tissue is made fluorescent. Subsequently, a region in the tissue is bleached using a high laser power. After bleaching, the bleached and unbleached fluorescent molecules will diffuse through the tissue. By recording the fluorescent intensity with a confocal microscope, the diffusion of the molecules can be determined by either analytical analysis (Braeckmans et al., 2003; Hauser et al., 2008; Soumpasis, 1983), Fourier analysis (Travascio et al., 2009; Tsay and Jacobson, 1991), or finite element analysis (Irrechukwu and Levenston, 2009; Sniekers and van Donkelaar, 2005). Numerical analyses have been previously presented that could account for both the inhomogeneity of the tissue (Sniekers and van Donkelaar, 2005) and anisotropic diffusion (Travascio et al., 2009; Tsay and Jacobson, 1991). These methods can be adapted for human skin.

To improve targeted drug delivery, the aim of present study was to determine the diffusion coefficient of two model compounds in human skin throughout its different layers. This was achieved using FRAP experiments in combination with finite element analysis. The diffusion of fluorescent dextran molecules with two different molecular weights was examined.

2. Methods

2.1 Preparation of human skin samples

Human skin with subcutaneous fat of 3 female patients, aged between 40 and 58 years, who had undergone abdominoplasty, was obtained from the Catharina Hospital, Eindhoven, the Netherlands, according to Dutch guidelines of secondary used materials. Within 4 hours post-surgery, the skin was transported to the host laboratory and processed. The surface of the skin was cleaned with ethanol and samples with an approximate surface area of 8 mm by 8 mm and a thickness of approximately 4 mm, including the epidermis, dermis and part of the subcutaneous fat, were prepared using a scalpel, surgical scissors and a punch. These samples were cut perpendicular to the skin surface using a cutting device designed and described by Grams et al. (Grams et al., 2004), creating a flat cutting plane. After removal from the cutting device, the samples were immerged in 0.8 mg/ml 40 kDa or 0.8-1.2 mg/ml 500 kDa fluorescein dextran (Molecular Probes) in Hank's balanced salt solution with 20 µg/ml Hoechst 33342 (Molecular Probes) and stored at 4℃ for at least 20 hours.

Before the FRAP experiments, samples were allowed to equilibrate to room temperature for at least 30 minutes. Each sample was patted dry with gauze and placed on a glass cover slip with the cutting plane facing downwards. A border of polydimethylsiloxaan (PDMS) of 5 mm in height was placed on the cover slip around the sample and covered with a moistened gauze to prevent dehydration of the skin.

2.2 FRAP protocol

FRAP experiments were performed at 8 different depths measured from the surface of the skin. The depths corresponded to the central epidermis (at approximately 50% of the epidermal thickness), the upper, central and lower papillary dermis (at 10, 50, and 90% of its thickness), and two upper, a central and a lower location in the reticular dermis (at 5, 10, 50 and 90% of its thickness). To identify these locations, the thickness of the stratum corneum, epidermis, papillary and reticular dermis was determined. For this, cell nuclei, stained with Hoechst, were excited and collagen fibres of the reticular dermis were visualized using second harmonic generation (Theodossiou et al., 2006). After a location was selected, it was centred and a global image of the nuclei and collagen fibres was made using a 10x/0.3 NA EC Plan-Neofluar objective (Fig 1a). Subsequently, 10 images were recorded using the same objective, but with a zoom factor of 10, to establish a mean value of each pixel over the targeted recovery area A_r. This was immediately followed by the FRAP experiment. A circular area with a diameter of 30 µm was bleached by an Argon laser with a wavelength of 488 nm at 100% laser power and 100% transmission. Subsequently, images of 128 x 128 pixels were recorded at a frequency of 4 Hz at 0.7% laser transmission to monitor the fluorescent recovery for 100 seconds, resulting in images with a resolution of 0.7 x 0.7 µm per pixel (Fig 1b). The recovery was recorded inside the sample at a depth of 40-50 µm from the flat cutting plane with a slice thickness of 19.9 µm. All experiments were performed with a confocal laser scanning microscope (LSM 510 Meta NLO, Zeiss, Germany) and within 50 hours after surgery.

2.3 Image post processing

The images of the FRAP experiments were first processed using MATLAB (2013a, The MathWorks, Inc., Natick, MA, USA) (Fig 2). Each postbleach image was subtracted from the mean intensity distribution of the 10 prebleach images to remove inhomogeneities caused by structural features in the skin. From this set of images, the average intensity of 3 x 3 pixels was taken to form a new set of images of 42 x 42 pixels. Subsequently, the temporal change in intensity of each pixel was filtered using a low-pass first order

Butterworth filter with a cutoff frequency of 0.08 Hz to reduce imaging noise. Because the intensity *I(x,y,t)* was linearly related to the concentration in the concentration range of the fluorescent probes, the final set of images provided the spatiotemporal change in the concentration distribution $C_{exp}(x,y,t)$.

2.4 Analysis of the diffusion coefficient using a finite element model

A FRAP experiment can be modelled by solving the diffusion equation for dextran (eq 1).

$$\frac{\partial C}{\partial t} = \nabla^2 (D\nabla C), \quad (1)$$

where C is the concentration of dextran dependent on the x and y coordinates, D the diffusion coefficient of dextran and t the time. In the current study, the diffusion coefficient was assumed to be constant within each region. Solving this equation was achieved by designing a two-dimensional finite element (FE) model (Fig 1c) simulating the FRAP experiments using Abaqus/Standard (v6-11.2, Dassault Systèmes Simulia Corp., Providence, RI, USA). By comparing the results of the FE simulation with the FRAP experiments, the diffusion coefficient at the various locations within the inhomogeneous skin was estimated (Fig 2), in a similar manner to that previously reported (Irrechukwu and Levenston, 2009; Sniekers and van Donkelaar, 2005). For all simulations, a finite element model comparable to the size of the global image was used. In the centre of this model, the mesh consisted of a regular element grid, representing the recovery area A_r that was monitored during the recovery phase (Fig 1b). In this area, the size of a single element corresponded to the size of a single pixel of the processed images. In the surrounding part of the mesh A_s, the element size increased with distance from the centre (Fig 1c). Linear quadrilateral elements (DC2D4) were used in the entire model.

The initial concentration in the simulation was based on the first postbleach image. During bleaching, diffusion of fluorescent dextran already occurs. Consequently, the initial postbleach concentration of unbleached molecules inside the bleached area is not equal to zero. Therefore, the first image after bleaching was used to determine the initial concentrations. For A_r, the initial concentration of the nodes in the model was assigned by interpolation between corresponding experimental concentration values $C_{exp}(x,y,0)$. The mean concentration of all pixels located more than one eighth of the width of the image (67.5 µm) from the centre of the image was assigned as the initial concentration for A_s ($C_{As,0} = \overset{1}{C}(\sqrt{x^2+y^2} > 67.5\,\mu m, 0)$). At the outer boundaries of the model, this concentration was prescribed as a constant boundary condition during the entire simulation.

From the global image of the experiment, the skin was manually divided into an epidermal, papillary dermal, reticular dermal, and subcutaneous fat layer, with an additional region containing the stratum corneum and the air surrounding the sample. Subsequently, each element in the model was assigned to the layer in which the centre of the element was located (Fig 1c). Then, the simulation was performed using the backward Euler method for time integration.

After running the simulation, the spatiotemporal change in the concentration distribution of the analysis $C_{sim}(x,y,t)$ was exported and compared with the experimental change in concentration $C_{exp}(x,y,t)$ by means of the sum of squared differences. By iteratively changing the diffusion coefficient in the simulation, the difference between C_{sim} and C_{exp} was minimized using the MATLAB optimization function *fminbnd*.

During the optimization process, the diffusion coefficient of the examined layer was iteratively adapted, while the diffusion coefficient of the other layers remained constant. The diffusion coefficient for both the stratum corneum and air, and subcutaneous fat was always assigned a value of 0 $\mu m^2/s$. The diffusion coefficient at different depths in the reticular dermis was determined first with the other layers assigned a value of 62 $\mu m^2/s$, based on a previously reported diffusion coefficient for human epidermis (Cornelissen et al., 2008). The mean value determined from the four locations within the reticular dermis was then assigned to the reticular dermis and used to estimate the diffusion coefficient of the papillary dermis. In a similar manner, the diffusion coefficient of the epidermis was subsequently determined. This procedure was repeated until the diffusion coefficient did not change by more than 1 percent compared to the previous iteration. In addition, to assess the influence of the order in which the different layers were fitted, the same procedure was adopted starting with the epidermis, followed by the papillary and reticular dermis. This resulted in a maximal difference of 0.12 percent.

A few criteria were used to determine if the combination of the experiment and fitting procedure was appropriate. Two criteria were directly related to the FRAP experiments:

- The mean intensity of the prebleached images should be 30 units or more
- The intensity at the outer region of the postbleach image should not decrease by more than 0.1

Two other criteria were related to the goodness of fit:

- The value that was minimized should be less than $5x10^4$
- The final value of D should not approach the limiting values for which the objective function *f* was minimized, equivalent to the absence of a minimum value. These limits were set between 0 and 300 $\mu m^2/s$

The adopted analysis was validated and the influence of various bleach parameters were assessed using experiments on agarose gels. Results can be found in the supplementary material.

2.5 Statistical analysis

To examine if there existed a significant effect of location in the skin and molecular weight of the dextran on the diffusion coefficient, a non-parametric Kruskal-Wallis test was conducted. This was followed by stepwise stepdown multiple comparisons to determine homogeneous subsets in the data. Statistical analyses were performed using SPSS (IBM SPSS Statistics 22, IBM Corp., Armonk, NY, USA). The statistical significance level was prescribed at 5 per cent.

3. Results

3.1 Intensity and concentration profiles of the experiment and model

FRAP measurements were performed at 8 locations within 7 samples for each of the two molecular weights. Based on the criteria for the quality of experiments, 78 measurements (70% of the total) were selected for further analysis. During fitting of some pilot experiments, it appeared that the overall diffusion process could best be fitted by two time constants. Accordingly, for subsequent analysis only the first 15 seconds were used to optimize the fit of the model to the experiments. An example of the fluorescent images and the corresponding values estimated from the model is shown in figure 3. A typical example of the temporal profile of the concentration from the experiment and the corresponding model is illustrated in figure 4. It should be noted that after fitting all experiments, 8 of the 78 experiments were discarded based on the criteria for the quality of the fit, including all those associated with 500 kDa dextran at 50% depth of the reticular dermis.

3.2 Diffusion coefficient

The diffusion coefficient from all the experiments ranged between 5 and 101 $\mu m^2/s$ (Fig 5). For 500 kDa dextran, the diffusion coefficient was approximately 8 $\mu m^2/s$ at all locations, with slightly higher median values in the papillary dermis compared to the other layers. With a median value of 20 $\mu m^2/s$, the diffusion coefficient of the 40 kDa was higher than the corresponding value for 500 kDa. The values of the diffusion coefficient varied minimally between the different locations in the dermis for 40 kDa dextran. It is also evident that the median diffusion coefficient of the epidermis was more than twice as

low as those measured in the papillary and reticular dermis for 40 kDa dextran, with values of 8, 21, and 21 $\mu m^2/s$, respectively.

Statistical analysis revealed a significant difference between the different experimental groups ($p < 0.05$). Post hoc multiple comparison revealed two subsets of the experimental groups which were significantly different from each other, corresponding to the two molecular weights of dextran, i.e. 40 kDa and 500 kDa. However, for the epidermal layer, the diffusion coefficients yielded similar values for both dextrans.

These results indicated that the molecular weight of the dextran did have a significant effect on the estimated diffusion coefficient, while the location within the skin had no significant effect.

Close examination of the data revealed that the measured 101 $\mu m^2/s$ was an outlier in the 40 kDa 10% reticular dermis group. Further examination of this particular case, showed a poor fit. However, this outlier did not influence the findings from the statistical analysis.

4. Discussion

To facilitate the design of drug delivery systems to administer drugs both intra- and (trans)dermally, the transport of macromolecules through the human skin must be established. FRAP experiments in combination with FE analysis enabled the diffusion coefficient to be estimated for two sizes of dextran molecules. Results for the diffusion coefficient yielded a two fold increase for 40 kDa dextran compared to 500 kDa, with median values of 20 and 8 $\mu m^2/s$, respectively. The diffusion coefficient was similar within and between the papillary and reticular dermis. However, the value in the epidermis was less than 50% of the values in the dermal layers for the 40 kDa dextran molecule.

The diffusion coefficient in the epidermis was approximately 8 and 7 $\mu m^2/s$ for 40 and 500 kDa dextran, respectively (Fig. 5). This value was considerably lower than 62 $\mu m^2/s$, which had been previously measured in human epidermis using 20 kDa dextran (Cornelissen et al., 2008). The relatively large difference in the value of the diffusion coefficient may result from the non-linear dependency of the diffusion coefficient on the molecular weight (Gu et al., 2004; Irrechukwu and Levenston, 2009). In addition, the difference may be reinforced by possible damage due to heat separation of the epidermis used by Cornelissen and co-workers (Cornelissen et al., 2008). The values for the dermis were comparable with the wide range of previously reported diffusion coefficient for relative small molecules in human dermis (190-300 Da) (Ibrahim and Kasting, 2010; Xing et al., 2009). In the current study, the diffusion coefficient of the epidermis was found to be lower than in the dermis for 40 kDa dextran

molecules, as reported in previous studies on murine and human skin (Raphael et al., 2013; Xing et al., 2009).

The values measured in this study for human skin were generally higher than those previously measured with skin from other species such as rat, mice and pig (Liu et al., 2013; Raphael et al., 2013; Wonglertnirant et al., 2010). Previously, it was shown that the diffusion coefficient gradually increased with depth in porcine and murine dermis (Liu et al., 2013; Raphael et al., 2013). This trend was not found in the present work on human dermis. These differences between previous and current studies suggest that the diffusion coefficient varies between species, and hence, has to be taken into account when studying transport in the skin.

The novelty of our experimental approach is the choice to image perpendicular to the skin surface, the way finite element simulations were used and the application of the method to human skin. Imaging across a plane corresponding to a cross section of the skin, enabled the determination of the diffusion coefficient in multiple layers using confocal microscopy. This would not have been possible when images were made parallel to the skin surface, since the imaging depth is limited in the thick human skin. In addition, FRAP is a convenient method to determine the diffusion coefficient of a range of fluorescently labelled molecules in various materials. For FRAP experiments, the entire sample is immersed in a fluorescent molecule. This can be a more controlled and easier to perform method for administration compared to local administration of a molecule in the sample using, for example, a microneedle, as reported by Raphael et al. (2013). To subsequently determine the diffusion coefficient from FRAP experiments, a finite element analysis was used. This has advantages compared to analytical analysis, which are limited as assumptions have to be made about the initial values of in the experiment. For example, in most analytical models it is assumed that no diffusion occurs during bleaching, which is clearly not the case. By contrast, the initial conditions in numerical models can be chosen more freely and therefore more accurately represent the experiments. Thus, using finite element analysis, it is possible to accommodate diffusion during bleaching, by employing the first image after bleaching as the initial condition for the analysis. In contrast to previous studies using a finite element analysis to determine the diffusion coefficient from FRAP experiments (Irrechukwu and Levenston, 2009; Sniekers and van Donkelaar, 2005), the current method could account for both inhomogeneous materials and all available spatial information as opposed to information from a few selected regions.

The approach adopted in the present study to determine values of diffusion coefficients is appropriate for other materials. However, some aspects of the experimental approach need to be considered. First, the measurements were performed using in vitro skin samples and therefore some

conditions might be different from the in vivo state. Indeed, excision of pre-stretched skin from the body will inevitable result in skin shrinkage, which could influence transport behaviour. In addition, in the present experiment, the diffusion was recorded at a depth of 40-50 µm from the cutting plane to circumvent the possible influence of damaged cells and fibres at this plane. Besides, the skin was fully hydrated during the experiments, which has the advantage that the conditions are the same for every measurement but, in some cases, may differ from the in vivo state. Second, pilot studies on agarose gels showed that the calculated diffusion coefficient was partly dependent on the bleach diameter (see supplementary material). For the FRAP experiments on skin, a fixed bleach diameter of 30 µm was used to eliminate its influence on the differences in diffusion coefficient found within and between skin layers. However, the absolute values may be slightly different. Both in agarose and in skin it appeared that more processes played a role in diffusion. The change in concentration in the first seconds (~15 sec) and the subsequent period could not be described by a single diffusion coefficient. Therefore, the first 15 seconds of the recovery were used during fitting. This phenomena may be caused by some interaction between the macromolecules and the skin, preventing part of the molecules to move around freely and thereby causing a delay in the resulting recovery of the fluorescent intensity.

The diffusion coefficients that were determined in the current study are relevant for future research on sensor technology, where small concentrations of molecules in the skin such as biomarkers are monitored, and targeted drug delivery in human skin to, for example, target specific cells in immunotherapy or vaccination. The data obtained with the current method can be used to accurately predict the distribution of a molecule through the skin after its administration and to predict the efficiency of different application methods. If a minimal variation in the diffusion coefficient is observed within a single skin layer, as reported in the current study for dextrans, the authors propose the use of a single value for the epidermal and a single value for the dermal layer, each dependent on the molecular weight of the molecule.

This study assessed the transport of macromolecules through and within various human skin layers by means of the diffusion coefficient. It was shown that the diffusion coefficient only minimally varied within and between skin layers, but was dependent on the molecular weight of the macromolecule. The data presented can be used for future research on targeted drug delivery in the skin and thereby facilitate in the improvement of current delivery devices and strategies. By specifically assessing human skin, differences in skin properties between species can be taken into account.

Acknowledgements

We would like to thank the Catharina Hospital in Eindhoven for providing skin tissue. This research is supported by the Dutch Technology Foundation STW, which is part of the Netherlands Organisation for Scientific Research (NWO), and which is partly funded by the Ministry of Economic Affairs (Project no. 11259).

References

Anissimov, Y.G., Zhao, X., Roberts, M.S., Zvyagin, A.V., 2012. Fluorescence recovery after photo-bleaching as a method to determine local diffusion coefficient in the stratum corneum. Int. J. Pharm. 435, 93–97. doi:10.1016/j.ijpharm.2012.01.055

Arora, A., Prausnitz, M., Mitragotri, S., 2008. Micro-scale Devices for Transdermal Drug Delivery. Int. J. Pharm. 364, 227–236. doi:10.1016/j.ijpharm.2008.08.032

Bal, S.M., Kruithof, A.C., Zwier, R., Dietz, E., Bouwstra, J.A., Lademann, J., Meinke, M.C., 2010. Influence of microneedle shape on the transport of a fluorescent dye into human skin in vivo. J. Controlled Release 147, 218–224. doi:10.1016/j.jconrel.2010.07.104

Braeckmans, K., Peeters, L., Sanders, N.N., De Smedt, S.C., Demeester, J., 2003. Three-Dimensional Fluorescence Recovery after Photobleaching with the Confocal Scanning Laser Microscope. Biophys. J. 85, 2240–2252. doi:10.1016/S0006-3495(03)74649-9

Chen, M.-C., Ling, M.-H., Lai, K.-Y., Pramudityo, E., 2012. Chitosan microneedle patches for sustained transdermal delivery of macromolecules. Biomacromolecules 13, 4022–4031. doi:10.1021/bm301293d

Chen, X., Fernando, G.J.P., Crichton, M.L., Flaim, C., Yukiko, S.R., Fairmaid, E.J., Corbett, H.J., Primiero, C.A., Ansaldo, A.B., Frazer, I.H., Brown, L.E., Kendall, M.A.F., 2011. Improving the reach of vaccines to low-resource regions, with a needle-free vaccine delivery device and long-term thermostabilization. J. Controlled Release 152, 349–355. doi:10.1016/j.jconrel.2011.02.026

Chen, X., Kask, A.S., Crichton, M.L., McNeilly, C., Yukiko, S., Dong, L., Marshak, J.O., Jarrahian, C., Fernando, G.J.P., Chen, D., Koelle, D.M., Kendall, M.A.F., 2010. Improved DNA vaccination by skin-targeted delivery using dry-coated densely-packed microprojection arrays. J. Controlled Release 148, 327–333. doi:10.1016/j.jconrel.2010.09.001

Cornelissen, L.H., Bronneberg, D., Oomens, C.W.J., Baaijens, F.P.T., 2008. Diffusion measurements in epidermal tissues with fluorescent recovery after photobleaching. Skin Res. Technol. 14, 462–467. doi:10.1111/j.1600-0846.2008.00313.x

Deschout, H., Raemdonck, K., Demeester, J., Smedt, S.C.D., Braeckmans, K., 2014. FRAP in Pharmaceutical Research: Practical Guidelines and Applications in Drug Delivery. Pharm. Res. 31, 255–270. doi:10.1007/s11095-013-1146-9

Fernando, G.J.P., Chen, X., Prow, T.W., Crichton, M.L., Fairmaid, E.J., Roberts, M.S., Frazer, I.H., Brown, L.E., Kendall, M.A.F., 2010. Potent immunity to low doses of influenza vaccine by probabilistic guided micro-targeted skin delivery in a mouse model. PLoS ONE 5, e10266. doi:10.1371/journal.pone.0010266

Gelinck, L.B.S., van den Bemt, B.J.F., Marijt, W.A.F., van der Bijl, A.E., Visser, L.G., Cats, H.A., Rimmelzwaan, G.F., Kroon, F.P., 2009. Intradermal influenza vaccination in immunocompromized patients is immunogenic and feasible. Vaccine 27, 2469–2474. doi:10.1016/j.vaccine.2009.02.053

Grams, Y.Y., Whitehead, L., Cornwell, P., Bouwstra, J.A., 2004. On-Line Visualization of Dye Diffusion in Fresh Unfixed Human Skin. Pharm. Res. 21, 851–859. doi:10.1023/B:PHAM.0000026439.63969.30

Gu, W.Y., Yao, H., Vega, A.L., Flagler, D., 2004. Diffusivity of Ions in Agarose Gels and Intervertebral Disc: Effect of Porosity. Ann. Biomed. Eng. 32, 1710–1717. doi:10.1007/s10439-004-7823-4

Hanh, B.D., Neubert, R.H.H., Wartewig, S., Lasch, J., 2001. Penetration of compounds through human stratum corneum as studied by Fourier transform infrared photoacoustic spectroscopy. J. Controlled Release 70, 393–398. doi:10.1016/S0168-3659(00)00371-0

Hauser, G.I., Seiffert, S., Oppermann, W., 2008. Systematic evaluation of FRAP experiments performed in a confocal laser scanning microscope – Part II: Multiple diffusion processes. J. Microsc. 230, 353–362. doi:10.1111/j.1365-2818.2008.01993.x

Ibrahim, R., Kasting, G.B., 2010. Improved method for determining partition and diffusion coefficients in human dermis. J. Pharm. Sci. 99, 4928–4939. doi:10.1002/jps.22216

Irrechukwu, O.N., Levenston, M.E., 2009. Improved Estimation of Solute Diffusivity Through Numerical Analysis of FRAP Experiments. Cell. Mol. Bioeng. 2, 104–117. doi:10.1007/s12195-009-0042-1

Liu, P., Huang, Y., Guo, Z., Wang, J., Zhuang, Z., Liu, S., 2013. Discrimination of dimethyl sulphoxide diffusion coefficient in the process of optical clearing by confocal micro-Raman spectroscopy. J. Biomed. Opt. 18, 020507–020507. doi:10.1117/1.JBO.18.2.020507

Pasparakis, M., Haase, I., Nestle, F.O., 2014. Mechanisms regulating skin immunity and inflammation. Nat. Rev. Immunol. 14, 289–301. doi:10.1038/nri3646

Prow, T.W., Chen, X., Prow, N.A., Fernando, G.J.P., Tan, C.S.E., Raphael, A.P., Chang, D., Ruutu, M.P., Jenkins, D.W.K., Pyke, A., Crichton, M.L., Raphaelli, K., Goh, L.Y.H., Frazer, I.H., Roberts, M.S., Gardner, J., Khromykh, A.A., Suhrbier, A., Hall, R.A., Kendall, M.A.F., 2010. Nanopatch‐Targeted Skin Vaccination against West Nile Virus and Chikungunya Virus in Mice. Small 6, 1776–1784. doi:10.1002/smll.201000331

Quan, F.-S., Kim, Y.-C., Compans, R.W., Prausnitz, M.R., Kang, S.-M., 2010. Dose sparing enabled by skin immunization with influenza virus-like particle vaccine using microneedles. J. Controlled Release 147, 326–332. doi:10.1016/j.jconrel.2010.07.125

Raphael, A.P., Meliga, S.C., Chen, X., Fernando, G.J.P., Flaim, C., Kendall, M.A.F., 2013. Depth-resolved characterization of diffusion properties within and across minimally-perturbed skin layers. J. Controlled Release 166, 87–94. doi:10.1016/j.jconrel.2012.12.010

Raphael, A.P., Prow, T.W., Crichton, M.L., Chen, X., Fernando, G.J.P., Kendall, M.A.F., 2010. Targeted, Needle‐Free Vaccinations in Skin using Multilayered, Densely‐Packed Dissolving Microprojection Arrays. Small 6, 1785–1793. doi:10.1002/smll.201000326

Scott, R.C., Corrigan, M.A., Smith, F., Mason, H., 1991. The influence of skin structure on permeability: an intersite and interspecies comparison with hydrophilic penetrants. J. Invest. Dermatol. 96, 921–925.

Sniekers, Y.H., van Donkelaar, C.C., 2005. Determining Diffusion Coefficients in Inhomogeneous Tissues Using Fluorescence Recovery after Photobleaching. Biophys. J. 89, 1302–1307. doi:10.1529/biophysj.104.053652

Soumpasis, D.M., 1983. Theoretical analysis of fluorescence photobleaching recovery experiments. Biophys. J. 41, 95–97. doi:10.1016/S0006-3495(83)84410-5

Theodossiou, T.A., Thrasivoulou, C., Ekwobi, C., Becker, D.L., 2006. Second Harmonic Generation Confocal Microscopy of Collagen Type I from Rat Tendon Cryosections. Biophys. J. 91, 4665–4677. doi:10.1529/biophysj.106.093740

Travascio, F., Zhao, W., Gu, W.Y., 2009. Characterization of Anisotropic Diffusion Tensor of Solute in Tissue by Video-FRAP Imaging Technique. Ann. Biomed. Eng. 37, 813–823. doi:10.1007/s10439-009-9655-8

Tsay, T.T., Jacobson, K.A., 1991. Spatial Fourier analysis of video photobleaching measurements. Principles and optimization. Biophys. J. 60, 360–368. doi:10.1016/S0006-3495(91)82061-6

Van der Maaden, K., Jiskoot, W., Bouwstra, J., 2012. Microneedle technologies for (trans)dermal drug and vaccine delivery. J. Controlled Release 161, 645–655. doi:10.1016/j.jconrel.2012.01.042

Wonglertnirant, N., Todo, H., Opanasopit, P., Ngawhirunpat, T., Sugibayashi, K., 2010. Macromolecular delivery into skin using a hollow microneedle. Biol. Pharm. Bull. 33, 1988–1993. doi:10.1248/bpb.33.1988

Xing, M.M.Q., Hui, X., Zhong, W., Pan, N., Yaghmaie, F., Maibach, H.I., 2009. In vitro human topical bioactive drug transdermal absorption: estradiol. Cutan. Ocul. Toxicol. 28, 171–175. doi:10.3109/15569520903097622

Fig 1. a) Global image of one of the FRAP experiments. The location for bleaching is in the centre of this image, represented by the red circle. The blue square represents the recovery area A_r, as visualized in figure b. Red represents collagen, cyan represents the cell nuclei, and green the fluorescein dextran. b) Example of a first postbleach image (recovery area A_r). The red circle represents the bleached area. c) The basic finite element mesh to simulate FRAP experiments. The mesh has the same size as figure a. In the recovery area A_r, the mesh is fine and has a regular grid. The size of this centre grid corresponds to the size of figure b. The colours indicate the different layers of the skin. Scale bars indicate 100, 10 and 100 µm for figure a, b, and c, respectively.

Fig 2. Flowchart describing the fitting procedure of a single experiment to determine the diffusion coefficient D of a location in the skin using finite element analysis.

Fig 3. The (change in) concentration (intensity) of a single experiment and results of the model fitted to the experiments. From top to bottom: postbleach images, postbleach images subtracted from the mean of the prebleach images, and the corresponding concentration profiles of the model (area A_r of the mesh is shown). From left to right: images at 0, 1 and 15 seconds after bleaching. The circle in the fluorescent images indicates the bleached area. The bars indicate 10 µm.

Fig 4. Comparison between a single experiment (postbleach images minus mean of prebleach images) and model fitted to this experiment. Each line represents the mean intensity of a circle with a width of 2.1 µm around the centre of the image. Note that because the intensities of the postbleach image were subtracted from the prebleach image a high difference in concentration represents the bleached area.

Fig 5. Distribution of the diffusion coefficient per location in the skin and molecular weight of the fluorescein dextran. The diffusion coefficient was significantly different for 40 and 500 kDa dextran. Each dot represents a single measurement. The black bar represents the median of the group. Note the broken y axis.

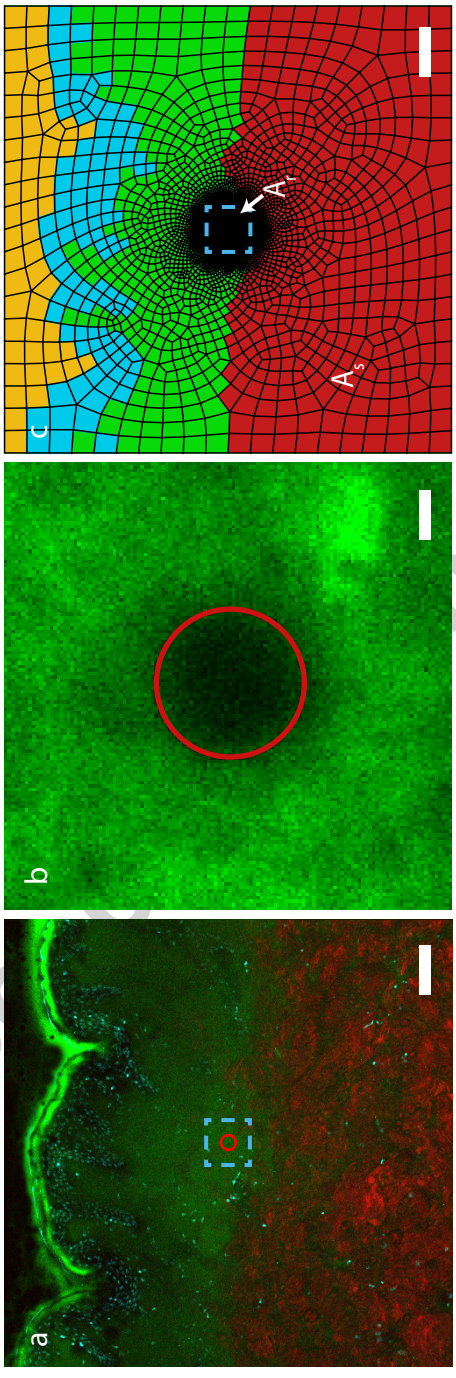

Figure1

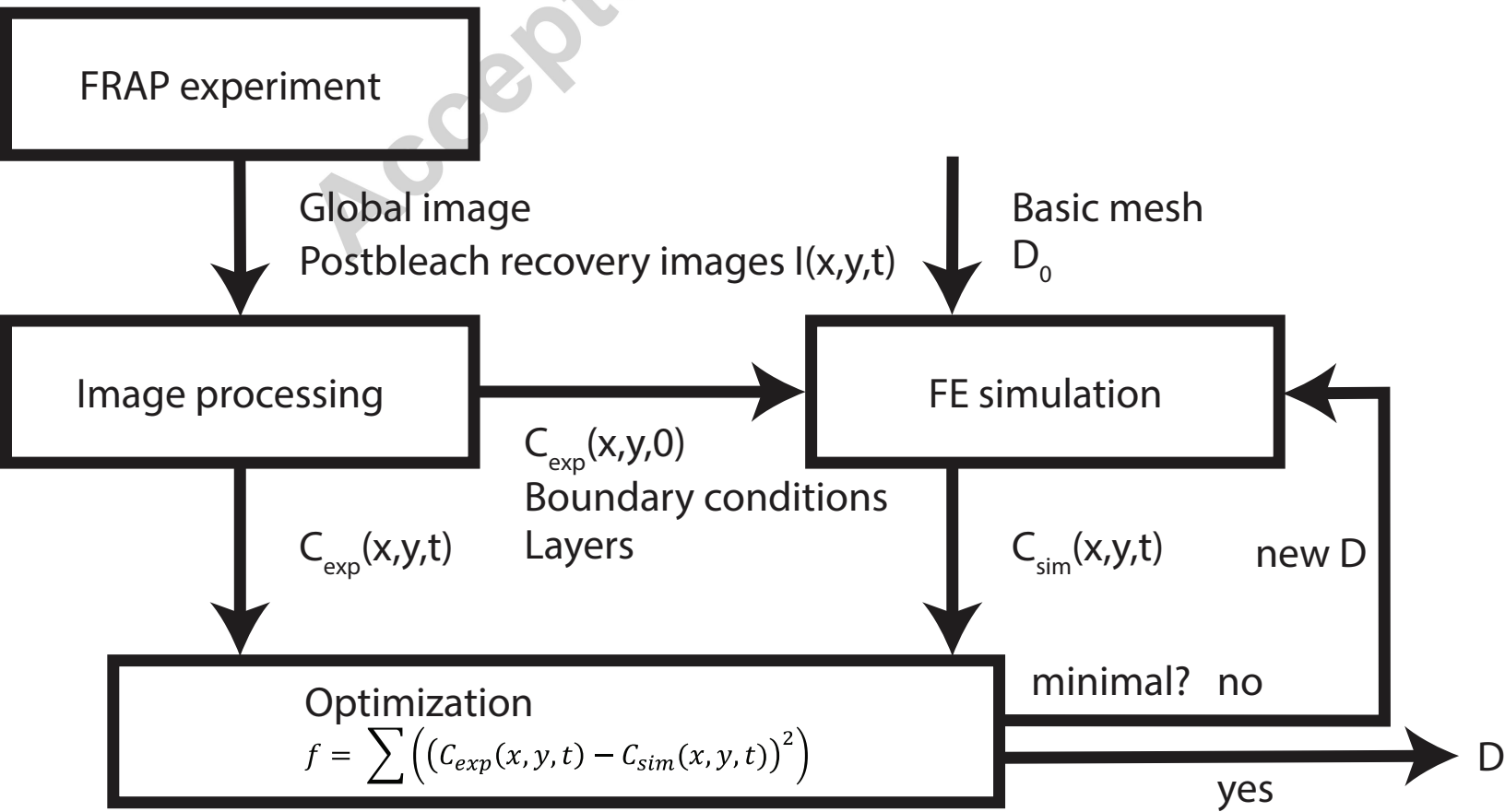

Figure3

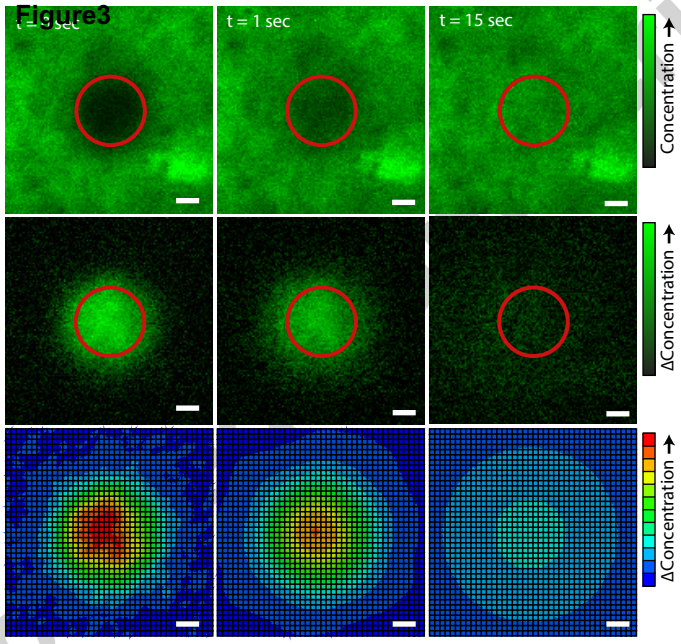

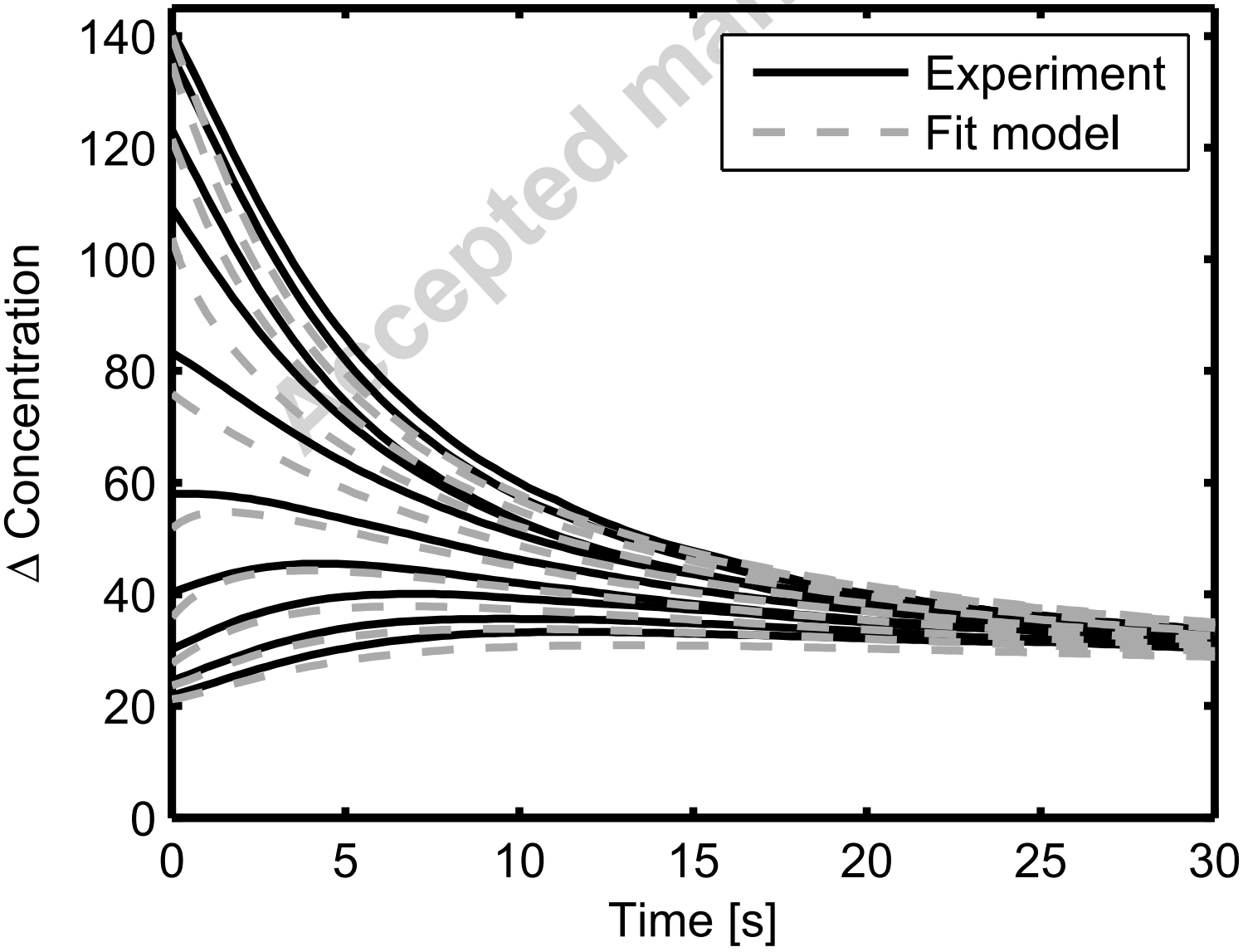

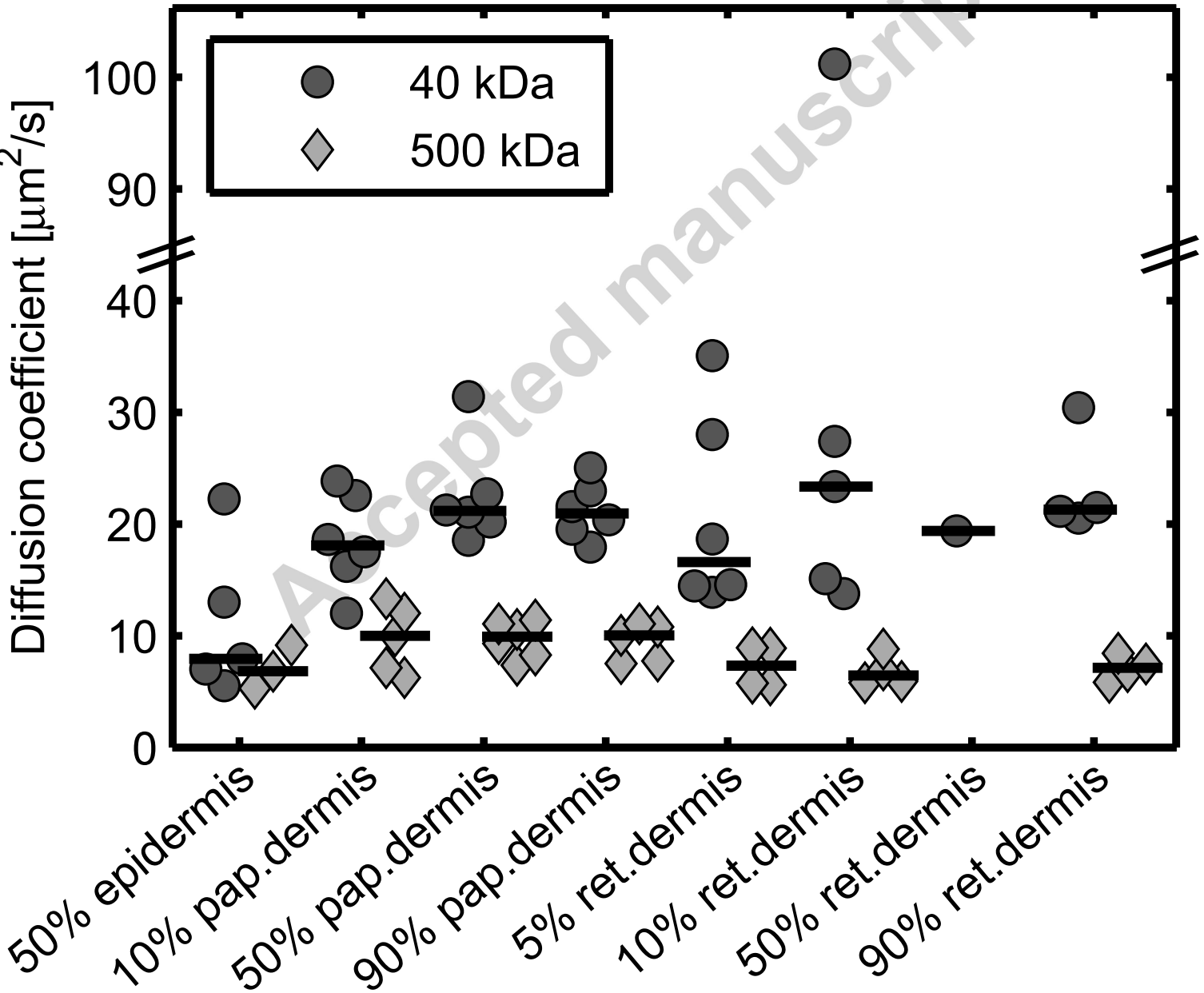

Highlights

- The diffusion coefficient was determined at various locations in the human skin
- Diffusion coefficients only slightly varied between different locations in the skin
- The diffusion coefficient was dependent on the molecular weight of the molecule